EXPERIMENTAL CHARACTERIZATION OF HIGH VISCOSITY DROPLET EJECTION

J. Mark Meacham[1] , Amanda O'Rourke[2], Yong Yang[3], Andrei G. Fedorov[1], F. Levent Degertekin[1], David W. Rosen[1]

[1] George Woodruff School of Mechanical Engineering, Georgia Institute of Technology, Atlanta, GA 30332-0405

[2]Boeing Unmanned Airborne Systems, Irvine, CA

[3]GE China Technology Center, Shanghai, China

Abstract

Additive Manufacturing via Microarray Deposition (AMMD) expands the allowable range of physical properties of printed fluids to include important, high-viscosity production materials (e.g., polyurethane resins). This technique relies on a piezoelectrically-driven ultrasonic print-head that generates continuous streams of droplets from 45 mm orifices while operating in the 0.5 to 3.0 MHz frequency range. Unique to this new printing technique are the high frequency of operation, use of fluid cavity resonances to assist ejection and acoustic wave focusing to generate the pressure gradient required to form and eject droplets. Specifically, we found that peaks in the ejection quality corresponded to predicted device resonances. Our results indicate that the micromachined ultrasonic print-head is able to print fluids up to 3000 mN-s/m^2, far above the typical printable range.

1 Introduction

Recent developments in inkjet printing methods have not kept pace with the evolution of printed materials, from inks deposited onto porous surfaces in the form of two-dimensional (2D) text or images to complex fluids used for the free-form fabrication of three-dimensional (3D), multilayer devices. Inkjet printing has a number of demonstrated advantages over conventional additive manufacturing (AM) technologies (e.g., stereolithography and laser sintering); unfortunately, the print-heads used in AM and other high resolution printing machines are restricted to materials with a limited range of physical properties. For example, viscosity is typically limited to below 40 mN-s/m^2 and surface tension to above 28 mN/m [1, 2].

1.1 Inkjet printing methods, materials and applications

Ink-jet printing has the promise of large-scale, economical manufacturing for a wide variety of polymer and, potentially, other materials. AM processes that are not printing-based are restricted to processing of materials at a single point. Conversely, printing-based methods are termed 'scalable' because the cost of adding more nozzles to an array is low. In addition, printing processes enable straightforward fabrication of multi-material parts and devices by dedicating different nozzles to different materials [1-3]. Although a number of droplet generation techniques are used in practice (see Le [4] for a thorough review), most AM systems utilize piezoelectric actuation. For example, MicroFab Technologies, Inc. (www.microfab.com, Plano, TX), FUJIFILM Dimatix, Inc. (www.dimatix.com, Santa Clara, CA), and Xaar, PLC (www.xaar.co.uk, Cambridge, UK) market print-heads that are capable of producing 30–100 μm diameter droplets from large nozzle arrays driven at piezoelectric pumping frequencies between 2 and 20 kHz.

Many printing-based AM systems are available. Solidscape, Inc. (formerly Sanders Prototype, Inc., www.solid-scape.com, Merrimack, NH) was first to commercialize a printer that utilized independent nozzles for wax-based part and support structure materials. 3D Systems (www.3dsystems.com, Rock Hill, SC) has introduced a number of printing-based machines (e.g., the Actua 2100 in 1997, and the ThermoJet, InVision and ProJet lines in 2001, 2003 and 2008, respectively) with ever-increasing array sizes that now exceed several hundred nozzles. Objet Geometries, Inc. (www.object.com, Billerica, MA) has introduced machines (e.g., the Alaris30, Connex500 and Eden family of printers) with several-hundred to thousands of nozzle print-heads. The ProJet line and the Objet systems define each cross-section of a part in a photopolymer, which is then cured by ultraviolet light between each printing pass. The Connex500 permits additional design complexity by printing two different materials, the relative concentrations of which can be adjusted to achieve varying properties. Although manufacturing parts using printing-based RP methods has proven to be fast and inexpensive, photopolymer materials and wax-based polymers do not possess the mechanical properties desired in most production applications; therefore, their usefulness is limited to prototype parts.

A wide variety of fluids (e.g., biomaterial suspensions, ceramic pastes and non-Newtonian polymers) are relevant to 3D printing applications. Demonstrating the ability to print simultaneously cells, cell aggregates and biodegradable supports has driven recent developments in tissue engineering [5-11]. Inkjet printing of conductive polymers and colloidal semiconductors is particularly useful for manufacturing flexible circuits [12], organic light emitting diodes (OLEDs) [13, 14], polymer photovoltaics [15] and transistors [3, 16]. A thorough introduction to conductive polymers in embedded electronic circuits and structural parts is provided by MacDiarmid [17]. Ainsley et al. [18] have printed ceramic alumina slurries with up to 40 percent solids (by volume) using wax and kerosene to reduce paste viscosity. Polyurethanes represent an important class of materials for production applications; however, relatively high viscosities (up to 10 N-s/m^2) hinder printing of urethane-based resins in conventional inkjet systems.

1.2 Micromachining as an enabling technology for printer development

Micromachining techniques are particularly well-suited to fabrication of arrays of uniform micron-sized orifices. As a consequence, the evolution of inkjet printing has been greatly influenced by developments in the area of micro-electromechanical systems (MEMS). The gradual reduction in nozzle orifice size and, as a result, droplet diameter from approximately 50 μm to less than 5 μm is the most obvious result of progress in microfabrication. For example, orifice plates have been created by electroforming a metal over a pattern of nonconductive photoresist islands, which dictate the location and size of 2–6 μm orifices (see for example [19]). Atomization from thin (tens of microns) electroformed nozzle plates is typically achieved by vibrating the plate at high frequencies (~10 kHz). Device actuation has also been achieved by using a pressurized reservoir to push liquid jets from an array of laser-drilled 2.5 μm diameter holes in a polymer film [20]. The jets subsequently broke up into droplets with a mean diameter (~2.9 μm) slightly larger than that of the orifice. Femtoliter-sized (~5 μm diameter) droplets were produced by de Heij et al. [21] and Yuan et al. [22, 23] using bending mode piezoelectric transducers operating at up to 200 kHz to actuate arrays of 5 μm diameter nozzles micromachined in 10–20 μm thick silicon membranes using deep reactive ion etching (DRIE). Perçin et al. [24-29] relied on a micromachined flextensional ultrasound transducer to excite the axisymmetric resonant modes in a clamped circular plate and periodically elevate the pressure within a fluid reservoir. If the pressure was high enough to overcome fluid inertia and surface

tension, a droplet was ejected. Droplet ejection was demonstrated for a number of orifices including some as small as 4 µm in a 100 µm diameter membrane driven at 3.45 MHz [24]. Although MEMS-based droplet generators exhibit a high degree of control over orifice uniformity and location, their fabrication processes are typically complex. Further, device robustness may be an issue in printing high-viscosity liquids.

1.3 Additive Manufacturing via Microarray Deposition (AMMD)

We propose a novel manufacturing technique termed Additive Manufacturing via Microarray Deposition (AMMD) that relies on a MEMS-enabled print-head to form and eject liquid droplets from arrays of micro-scale (3–50 µm) nozzles [25, 26]. Ultrasonic actuation, resonant operation and acoustic wave focusing combine to enable efficient deposition of materials that conventional print-heads are unable to print. The high frequency of operation (0.5–3 MHz) and parallel (array) format make possible fast deposition of large volumes of material. Further, multi-material structures can potentially be created by utilizing different reservoirs driven by one or more piezoelectric transducers. The piezoelectric transducer operating frequency is matched to specific cavity resonant frequencies in order to efficiently transfer power from the piezoelectric transducer to acoustic waves within the sample reservoir. The pressure gradient required to print even high-viscosity materials is realized by exploiting the acoustic wave focusing properties of liquid horn structures. We demonstrate the ejection of liquids with a range of surface tensions (~25–73 mN/m) and viscosities (0.7–3000 mN-s/m^2); a qualitative judgment termed 'jettability' is used to compare ejection of different liquids (e.g., water, glycerol-water mixtures and a urethane-based photopolymer resin).

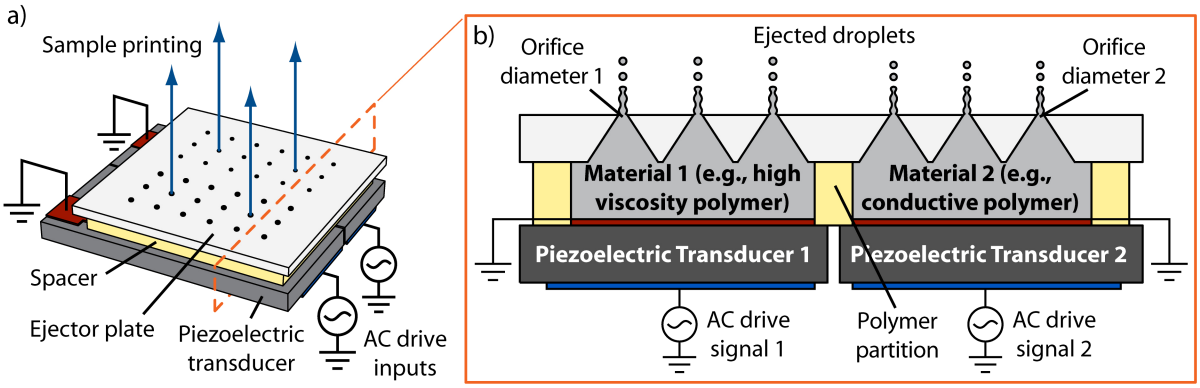

Figure 1. Schematic of the AMMD printer (not to scale). a) Two-fluid multiplexed printer assembly including ejector microarray with two orifice sizes and b) cross-section of the print-head assembly.

2 Print-Head Design

The AMMD printer schematic shown in Fig. 1 illustrates its most basic multiplexed embodiment with two individually-actuated compartments. The device comprises a piezoelectric transducer for ultrasound wave generation, a reservoir for storing materials to be printed and a set of acoustic horn structures, terminated by microscopic orifices, which form a nozzle array for focused application of mechanical stimuli at the nozzle tips. Each compartment is loaded with the different fluids needed for fabrication of a multi-material part. When either chamber of the device is driven at a particular resonant frequency of the liquid horn structures, acoustic waves within the sample chamber are focused by the horns. The two sets of nozzles shown in Fig. 1 are also terminated by two different orifice sizes allowing for easier implementation of multi-scale

part manufacturing. The realized ejector microarray consists of a rectangular fluid reservoir sandwiched between a lead zirconate titanate (PZT-8) piezoelectric ceramic (P880, American Piezo Ceramics, Inc.) and a silicon cover plate into which the ejector nozzles are micromachined. The pyramidal shape of the nozzles, which is suitable for focusing acoustic waves, is readily fabricated via anisotropic potassium hydroxide (KOH) wet etching of lithographically patterned [100]-oriented single crystal silicon.

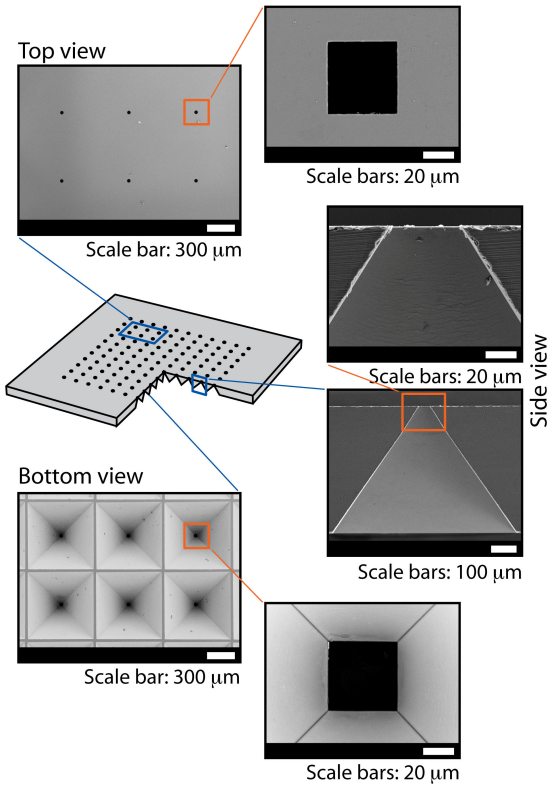

Figure 2. Scanning electron microscope (SEM) images of silicon (Si) microarrays used in the ejection experiments, with 45 μm square orifices.

3 Methodology

3.1 Microarray fabrication

A detailed description of ejector microarray fabrication in silicon (Si) is provided by Meacham et al. [26]. A simplified version of that process was used to create pyramidal nozzles in Si microarrays for use in the experiments described herein. In brief, the process consisted of four steps: (1) silicon nitride (Si_3N_4) was deposited over the front and back sides of a [100]-oriented single crystal Si wafer, (2) an array of squares was etched through the Si_3N_4 on one side of the wafer using a reactive ion etch (RIE) (SLR Series Dual ICP, Plasma-Therm), (3) a potassium hydroxide (KOH) solution (45 weight-percent at 75 °C) (VWR, Westchester, PA) was used to anisotropically etch pyramidal nozzles into the Si wafer, and (4) the remaining Si_3N_4 was removed using buffered oxide etchant (BOE) (VWR, Westchester, PA). The Si_3N_4 layer served as a protective mask during the anisotropic wet etch of the Si, and the square pattern controlled the size of the resulting pyramids. The fabrication process parameters were adjusted such that each nozzle terminated in a microscopic square orifice.

Figure 2 provides scanning electron microscope (SEM) images of a realized ejector microarray. The shape of the nozzles was dictated directly by the KOH wet etch, which yielded 45 μm side length square orifices on the opposite side of the wafer. The cross-section of the nozzle clearly illustrates the geometry of the slanted sidewalls, which lie at an angle of 54.74° to the (100) surface of the Si wafer. The silicon plate measures 24 mm on a side with 400 nozzles located in a 20×20 array on an approximately 0.75 mm pitch.

3.2 Experimental setup

Evaluation of the AMMD technique was performed using an experimental setup similar to that previously reported for high-resolution visualization of the ejection process [25, 26]. A schematic of the fully-assembled test fixture is shown in Fig. 3a-b. The silicon ejector microarray was bonded to a plastic support plate with epoxy. The plastic plate was created in Renshape SL-7510 resin (Huntsman Advanced Materials Americas, Los Angeles, CA) using a

stereolithography process (Viper Si^2 SLA Machine, 3D Systems, Valencia, CA). The 2 mm thick piezoelectric transducer (P880, APC International, Mackeyville, PA) was likewise affixed to an aluminum support block, which allowed for efficient heat removal during high-power-input operation. A circular Teflon® gasket was placed between the plastic plate and aluminum block to define the sample reservoir between the microarray and piezoelectric transducer. For all experiments, the height of the reservoir was between 1 and 2 mm. A large barrel syringe was used to fill the reservoir prior to operation. The piezoelectric transducer was driven by a sinusoidal AC voltage signal that was supplied by a function generator (Model DS345, Stanford Research Systems, Sunnyvale, CA). The signal was amplified using an RF amplifier (Model AG1020, T&C Power Conversion, Rochester, NY). The function generator provided control of the frequency f and amplitude V_{fg} of the driving signal, as well as the number of pulses n and pulse frequency (period) $f_{d.c.}$ ($P_{d.c.}$) when operating at less than 100% duty cycle. Signal gain *amp.* was set using the amplifier. A type T thermocouple (Omega, Stamford, CT) was used to continuously monitor the temperature on the back surface of the transducer.

Successful ejection of high-viscosity liquids (e.g., glycerol-water mixtures and photopolymer resins) required significant power input to the piezoelectric transducer. Under these conditions, high electrical current and physical displacement of the piezoelectric transducer led to increased resistive and frictional losses. During ejection of photopolymer resins, the entire test fixture was lowered into a temperature-controlled water bath to avoid excessive heating and maintain the desired operating temperature within the sample reservoir.

3.3 Sample preparation and property determination

Although many fluids have been ejected using our printing system, we will focus on aqueous glycerol mixtures and a representative photopolymer resin with urethane oligomers (Albany International Corporation, Albany, NY) for this paper. Aqueous glycerol mixtures with a range of fluid properties (e.g., surface tension and viscosity), as well as a photopolymer resin that is representative of materials of interest in AM, were used as operating fluids. Because glycerol is completely miscible with water, it is well-suited to investigation of viscous effects in fluid flow problems. Glycerol-water mixtures of 0, 65, 85, 90, 92, 96 and 100 weight-percent were prepared from water and 99.7% pure glycerol (Fisher Scientific, Fair Lawn, NJ). Although surface tension σ plays an important role in the ejection process, its variation (~25–73 mN/m) was small relative to that of the dynamic viscosity μ (~0.7–3000 mN-s/m^2) for these mixtures over the range of experimental conditions (i.e., temperature $T < 60$ °C). Finally, the fluid compositions that were required to achieve a good spread in viscosity and surface tension data also exhibited a range of sound transmission speed c (~1400–1950 m/s), which plays a significant role in the optimal operating frequency of a print-head loaded with a given fluid.

Glycerol-water mixtures have been thoroughly characterized in the literature; therefore, the properties of the above mixture compositions were taken from tabulated data (surface tension and speed of sound) and an empirical formula derived from multiple property databases (viscosity). Viscosities at temperature varied from 15 to 625 mPa-s. At printing temperature of 40 °C the viscosity of pure glycerin was 326 mPa-s.

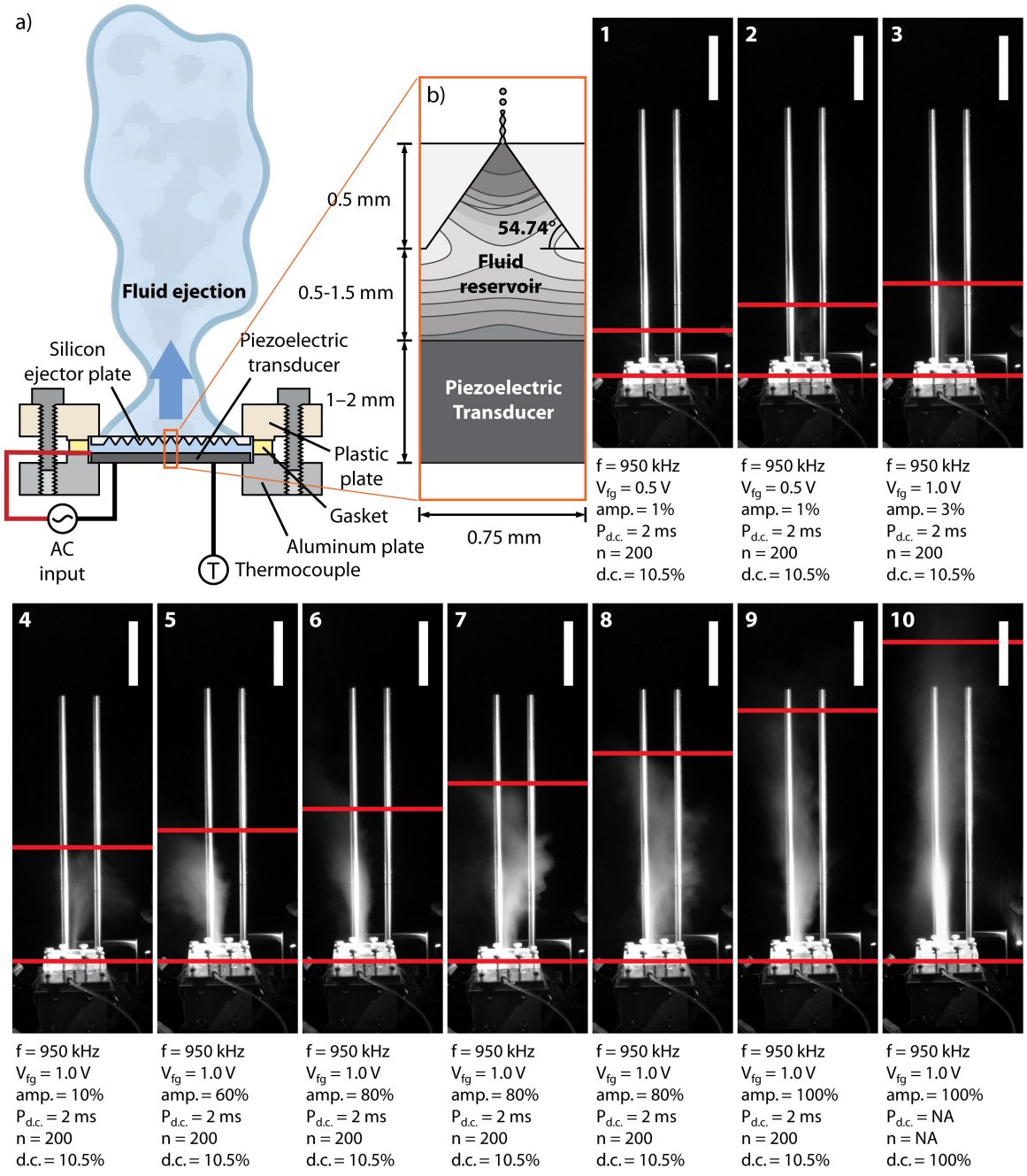

Figure 3. Experimental setup: a) schematic of the test fixture highlighting integral components and b) detail providing nominal dimensions of the microarray assembly. Jettability: the still photographs define a qualitative assessment tool for evaluating ejection capability. Scale bars are 10 cm.

Because no information is available in the literature, the fluid properties (e.g., surface tension, speed of sound and viscosity) of the urethane photopolymer were measured experimentally, as functions of temperature when possible. A modified version of the drop-weight-volume method originally introduced by Harkins and Brown [36, 37] was used to estimate the surface tension. Estimated surface tension values produced by this method included water (ρ = 1000 kg/m^3) σ = 70.1 mN/m, glycerol (ρ = 1260 kg/m^3) σ = 58.7 mN/m, and polydimethylsiloxane (PDMS) (ρ

= 970 kg/m^3) was σ = 21.6 mN/m. Considering the error associated with the determination of the average droplet volume, these values are extremely accurate. The surface tension of the photopolymer resin was found to be 29 mN/m. Although, measurements were only conducted at room temperature, the results provide an estimate of the photopolymer resin surface tension, which lies within a range bounded by the other reference fluids.

The speed of sound within the photopolymer resin was also determined using an in-house experimental setup. A plastic container that measured 11 mm on a side was filled with the sample liquid. The plastic container was then placed in a temperature controlled water bath. An ultrasonic transducer was driven at 7.5 MHz by a pulser-receiver (Panametrics 5072PR, Olympus NDT, Waltham, MA), which generated a sound wave that travelled through the liquid perpendicular to the container. The echo times for reflections from the front and back faces of the container were recorded by the receiver. The distance traveled (22 mm) was then divided by the time difference to obtain the speed of sound within the photopolymer resin. The speed of sound as a function of temperature T varied almost linearly from 1525 at 25 °C to 1390 at 65 °C.

A cone-plate rheometer (Physica MCR300, Anton-Paar GmbH, Graz, Germany) was used to evaluate the viscosity of the photopolymer resin. In order to confirm that the high-viscosity liquid was a Newtonian fluid, the viscosity was monitored while varying the shear rate γ at a constant temperature of 50 °C. The shear rate was increased from 0.01 to 100 s^{-1} in 20 steps and brought back to 0.01 s^{-1} in 10 steps. As indicated in Fig. 4a, the fluid retained its Newtonian character throughout the range of shear rates that were investigated. Note that the deviation from Newtonian behavior observed at low shear rates was due to limitations of the rheometer and not to the fluid itself. The viscosity was also measured as a function of increasing and decreasing temperature between 25 and 65 °C. Figure 4b is a plot of the average viscosity of four data sets (two increasing and two decreasing) over the temperature range of interest. Note that the maximum error for all average viscosity measurements was 1.5%. A 4th-order polynomial that was fit to the data is also shown in Fig. 4b. The reported viscosity for all subsequent experimental conditions was determined using this relationship.

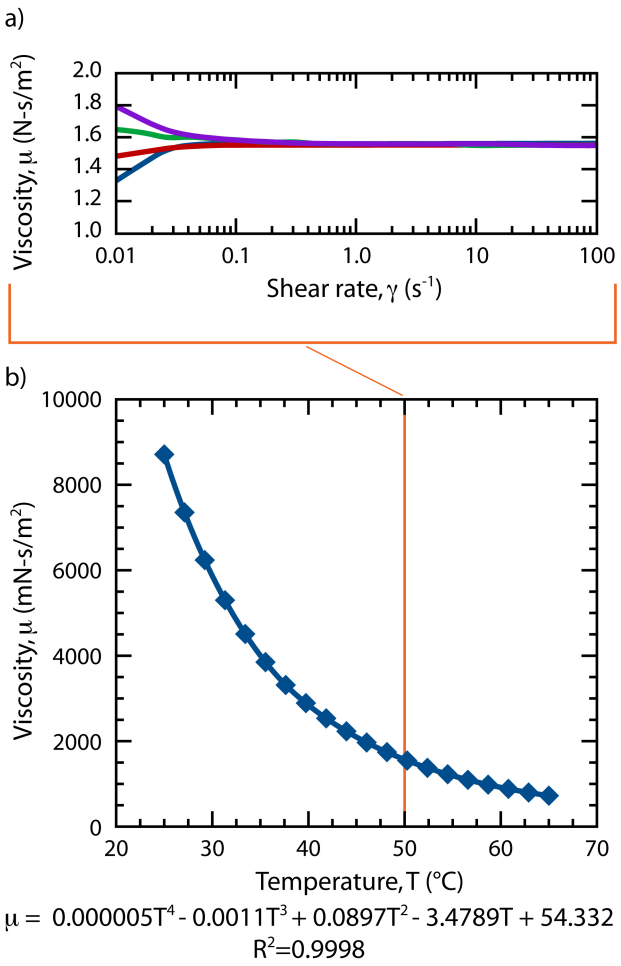

Figure 4. Viscosity μ for the urethane photopolymer resin: a) Viscosity as a function of shear rate γ and b) temperature T.

3.4 Assessment of printing capability

We evaluated the ability of the AMMD technique to print a particular fluid by

making a qualitative assessment of fluid atomization and comparing the observed performance to a reference scale. The still photographs shown in Fig. 3 were taken during water ejection under a range of operating conditions, which are provided below each photograph. The measured height of the plume and an estimate of the number of active nozzles were used to evaluate ejection quality on a scale of 1 to 10. The camera was unable to capture operation at the low end of the scale with steady, but weak, ejection from only 3 to 5 orifices; however, at peak performance, the device demonstrated jet ejection from more than 200 nozzles generating a large plume approximately 50 cm in height (see Fig. 3).

4 Results and Discussion

4.1 Jettability as a function of frequency

The acoustic responses of water and fuel-loaded ejector microarrays have previously been investigated using the harmonic analysis package of the commercial finite element analysis code ANSYS [38, 39]. These simulations indicated which frequencies corresponded to optimal device operation from both an efficiency standpoint and to achieve maximum power transfer from the piezoelectric transducer to generated droplets; however, the increase in operating temperature associated with operation at high electrical current and physical displacement of the piezoelectric transducer near resonance was not addressed. This phenomenon is particularly important for printing of high-viscosity fluids, which exhibit large changes in viscosity with only a slight increase in temperature.

In order to determine the relationship between operating frequency and ejection quality for high-viscosity fluids, the 'jettability' J_{ab} of glycerol-water mixtures with increasing weight-percent glycerol was evaluated. Figure 5 provides plots of J_{ab} as a function of frequency for 65, 85, 90, 92, 96 and 100 weight-percent glycerol. For all cases, the device was operated at less than 100% duty cycle with a pulse frequency $f_{d.c.}$ of 500 Hz and a pulse count n of 200. The signal gain *amp.* was set to 100%, and the amplitude V_{fg} of the driving signal was adjusted in order to achieve an observable increase in 'jettability' at the optimal ejection frequency. For example, $V_{fg} = 1$ V was adequate to achieve $J_{ab} = 9$ for 65% glycerol at $f = 950$ kHz; whereas, $V_{fg} = 10$ V was necessary to achieve only $J_{ab} = 7.5$ for 100% glycerol at the same operating frequency.

In general, the results shown in Fig. 5 follow the rough guideline for device design previously reported by Meacham et al. [39]. Fluid cavity resonances f_c are approximately related to the reservoir centerline height h_c and the speed of sound c within the ejection fluid as $f_c \approx m\, c/(2\kappa h_c)$ where m is the particular resonant mode. The reservoir height must be adjusted by the factor κ to account for the actual path length between the face of the piezoelectric transducer and the pressure wave focal point. For the first and second cavity resonant modes, the correction factors were reported as 0.77 and 0.93, respectively [39]. For 65% glycerol ($c = 1800$ m/s), peaks in 'jettability' are found at frequencies of 550 and 950 kHz, which are very near the predicted resonant frequencies of 580 and 970 kHz (note height h is 2 mm). As the weight-percent glycerol increases, only a slight shift of the resonant frequencies to to higher frequencies is seen. Although the speed of sound in pure glycerol is 10% greater than that in 65 weight-percent glycerol in water at room temperature (approximately 1950 vs. 1800 m/s), it is possible that the observed increase in operating temperature with glycerol concentration mitigates this effect somewhat.

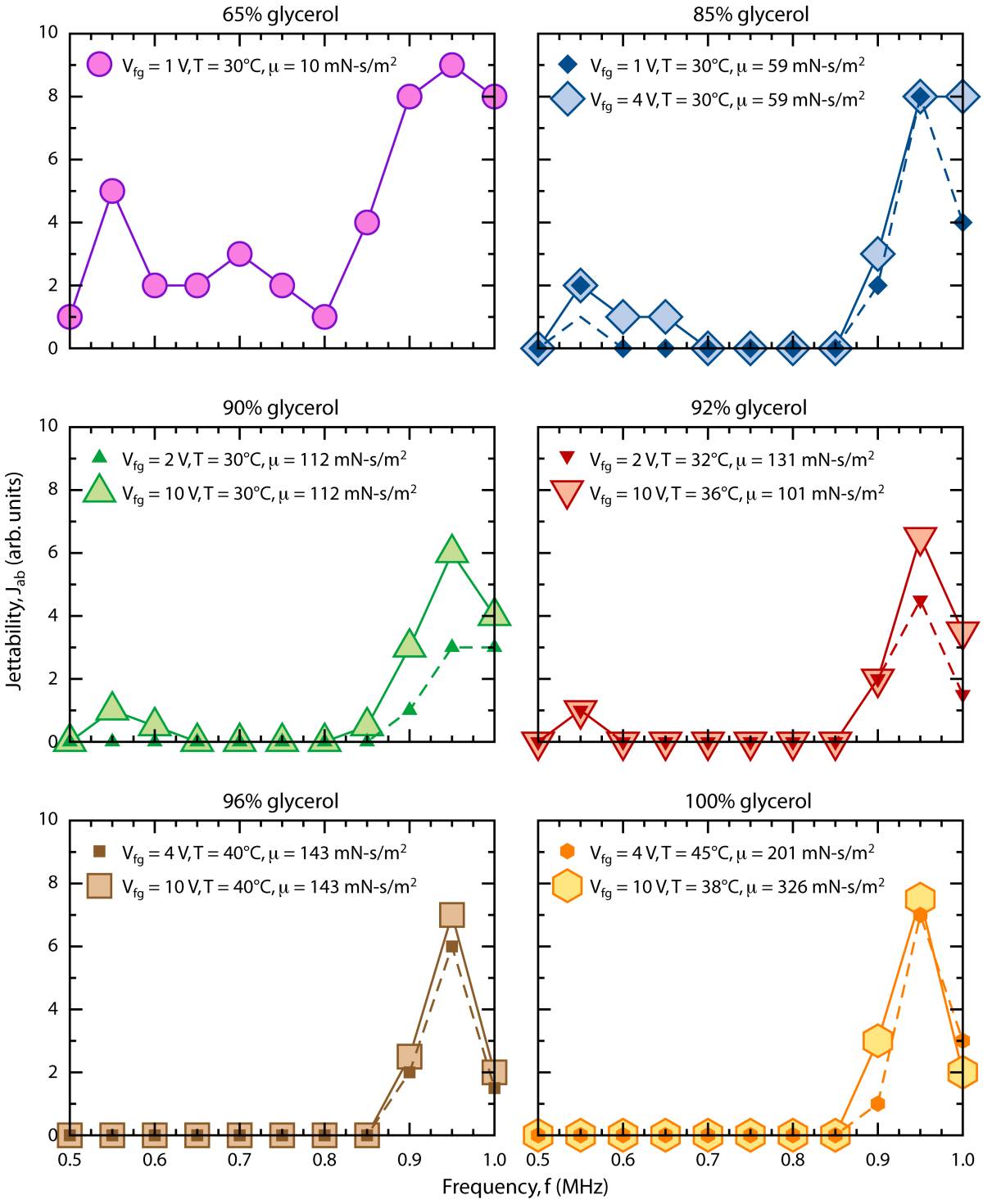

Figure 5. Jettability J_{ab} as a function of operating frequency f for glycerol-water mixtures with increasing weight-percent glycerol. For all cases, the device was operated at less than 100% duty cycle with a pulse frequency $f_{d.c.}$ of 500 Hz and a pulse count n of 200.

It is clear from Fig. 5 that increasing the viscosity of the operating fluid is detrimental to the quality of ejection. As the glycerol concentration is increased from 65 to 100%, with a corresponding increase in viscosity from 10 to 326 mN-s/m^2, 'jettability' at the first resonant frequency decreases quickly until all activity ceases at above 96 weight-percent glycerol. Although 'jettability' does not vanish entirely at the second resonance, the frequency envelope over which ejection can be achieved is significantly reduced for higher-viscosity mixtures. It is possible that the decrease in surface tension from 67 to 61.5 mN/m corresponding to the change in conditions represented by the data in Fig. 5 contributes to the drop in device performance; however, it is not likely that this has as significant an impact as the greater than one order-of-magnitude increase in viscosity.

4.2 Jettability as a function of duty cycle

Jettability was also investigated while varying the pulse count n of the signal driving the piezoelectric at a constant operating frequency f of 950 kHz and pulse frequency $f_{d.c.}$ of 500 Hz. Figure 6 is a summary of results for mixtures with 65, 85, 90, 92, 96 and 100 weight-percent glycerol. As before, the signal gain *amp.* was set to 100%, and the amplitude V_{fg} of the driving signal was adjusted in order to achieve observable changes in 'jettability' as the pulse count was decreased from 100 (duty cycle = ~0.05) to zero. As expected, the general trend displayed in Fig. 6 is a gradual increase in 'jettability', which appears to approach a maximum value beyond n = 100. More interesting is the ejection behavior as the pulse count approaches zero; even at duty cycles as low as 0.0025 (n = 5), faint ejection was observed. This result indicates that a small number of cycles is required to establish a favorable pressure field for ejection within the fluid reservoir.

The present system represents a driven, damped harmonic oscillator for which the quality factor Q of a resonance is expressed as

$$Q = \frac{\tau \omega_o}{2} \qquad (1)$$

where τ is the rise time for pressure wave amplitude to reach 1 – 1/e = 0.63 of its steady state value and ω_o is the angular frequency at resonance [40]. For high-Q systems, the quality factor can also be defined in terms of the full-width at half-maximum of the amplitude

$$Q = \frac{\omega_o}{\Delta \omega} \qquad (2)$$

where $\Delta\omega$ is the angular frequency difference at half of the maximum signal

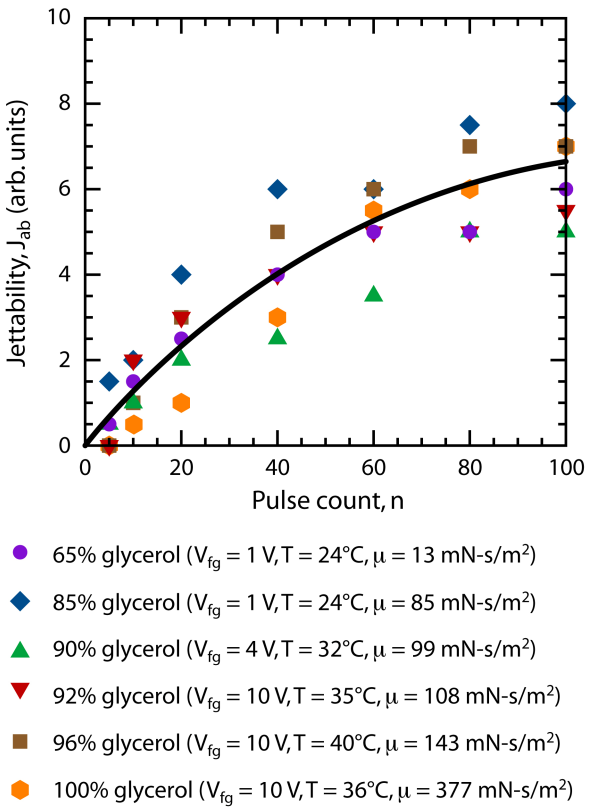

Figure 6. Jettability J_{ab} as a function of pulse count n for glycerol-water mixtures with increasing weight-percent glycerol. For all cases, the operating frequency f was 950 kHz, and the pulse frequency $f_{d.c.}$ was 500 Hz.

amplitude at resonance. Solving for τ in terms of frequency

$$\tau = \frac{1}{\pi \Delta f}. \qquad (3)$$

Based on Fig. 5 and results reported earlier by Meacham et al. [39], the frequency difference at half-maximum for a resonant frequency of 950 kHz is between 50 and 100 kHz. Substituting into equation (3), the rise time should be approximately 5 μs, which corresponds to five pulses of the signal driving the piezoelectric. This simple analysis provides an upper limit on the minimum number of pulses required to initiate ejection and indicates that the conclusions drawn from Fig. 6 are realistic.

4.3 Maximum and sustained jettability

In order to obtain the results shown in Figs. 5 and 6, the device was only operated for 5–10 s to evaluate the printing potential under the reported experimental conditions. Incorporating the microarray into a commercial print-head will require both demonstration of a high deposition rate, which is related to maximum achievable 'jettability', and continuous operation. As before, glycerol-water mixtures with 65, 85, 90, 92, 96 and 100 weight-percent glycerol were evaluated. Sustained ejection was only observed at the first resonance for 65% glycerol. At an operating frequency of 550 kHz (*amp.* = 100%, V_{fg} = 1 V, n = 100 and $f_{d.c.}$ = 500 Hz), ejection at J_{ab} = 6 was achieved for 90 s at an operating temperature T of 35 C. For all other mixtures at the first resonant frequency (~550 kHz), either sustained ejection was not possible, or the rise in operating temperature associated with prolonged operation was unacceptable.

Devices driven at the second resonant frequency (~950 kHz) exhibited more stable operation. The 'jettability' of 65% glycerol remained steady at J_{ab} = 8 for 86 s at T = 35 °C (*amp.* = 100%, V_{fg} = 1 V, n = 100 and $f_{d.c.}$ = 500 Hz). As the weight-percent glycerol was gradually increased from 85 to 90, 92, 96 and 100%, it was necessary to increase the amplitude V_{fg} of the signal driving the piezoelectric transducer from 1 to 5 V to achieve a reasonable 'jettability'. Over this range of mixture compositions, the 'jettability' slowly dropped from 8 to 4.5. For all but one of these cases, ejection was sustained for more than 70 s. The decrease in performance is attributed in part to a corresponding reduction in pulse count, which was necessary to control the temperature; however, even at n = 40, the steady state operating temperature rose to as high as 50 °C for the mixtures under investigation. Based on these results (mixture compositions and operating temperatures), the maximum viscosity for sustained ejection was approximately 150 mN-s/m^2. Finally, note that a 'jettability' of 10 (or the scale maximum from Fig. 3) was achieved for 65, 85, 90, 92, 96 and 100 weight-percent glycerol at operating temperatures of 35, 40, 56, 54, 63 and 70 °C, respectively, and a frequency of 950 kHz.

4.4 Ejection of photopolymer resin

The potential of AMMD for 3D inkjet printing was evaluated using the urethane photopolymer resin. Based upon the measured speed of sound (between 1400 and 1450 m/s over the range of operating temperatures, 40–60 °C) and using the same geometry as before, the first two resonant frequencies were estimated to be 500 and 900 kHz. Stable ejection was not possible at either frequency; however, sustained 'activity' was observed over 50 kHz windows at approximately 510 and 920 kHz (see Fig. 7c). In order to achieve observable jet ejection, it was necessary to clean the front face of the ejector microarray with methanol, which was allowed to evaporate before switching on the amplifier. Ejection was short-lived (~0.5 s) as fluid would quickly begin to weep from the nozzle orifices and form a thin layer, which would continue to oscillate. Figure

7 provides images of the experimental setup after cleaning, immediately after turning on the device, and after a period of weeping (10–15 s). The inability to sustain ejection is not thought to result from the increase in fluid viscosity, but from the decrease in surface tension reported in the *Methodology* section above. Similar behavior has been reported for atomization of hydrocarbon fuels (e.g., kerosene and methanol) [39]. Deposition of pink fluid onto a white cloth was used to confirm that the short burst of ejection was indeed photopolymer resin (and not methanol). Although not particularly remarkable, these results are encouraging, and represent the first successful attempt to print a photopolymer resin with such a high viscosity (~3000 mN-s/m^2).

4.5 Printing Indicator (p.i.)

Several investigators have identified a dimensionless parameter termed the 'printing indicator' (p.i.) that can be used to predict the printing potential of a given fluid [41]. The p.i. is defined as the ratio of the Reynolds number to the square root of the Weber number [p.i. = $\mathrm{Re}/\mathrm{We}^{1/2} = (\rho\, r\, \sigma)^{1/2}/\mu$] and is really just the inverse of the better known Ohnesorge number Oh. For successful printing, it is recommended that the p.i. be kept within a range of 1 to 10 [18]; however, as shown in Fig. 8, the proof-of-concept AMMD experiments conducted with glycerol-water mixtures and the representative photopolymer resin fall outside of this range. Aside from a small number of data points taken while operating at relatively high temperature (> 60 °C) or at low glycerol concentration, the demonstrated ejection of glycerol-water mixtures occurred for fluid viscosities of greater than 80 mN-s/m^2. The fluid properties of the urethane photopolymer resin (low surface tension and high viscosity) suggest that it is impossible to print, yet short-lived droplet generation was achieved at surface tensions below 30 mN/m and viscosities up to 3 N-s/m^2 (note the lower bound on the surface tension envelope in Fig. 8 is estimated based on the behavior of other fluids; surface tension of the photopolymer resin was not measured as a function of temperature). These preliminary results indicate that the ejector microarray is capable of printing fluids with much higher viscosities than conventional print-heads.

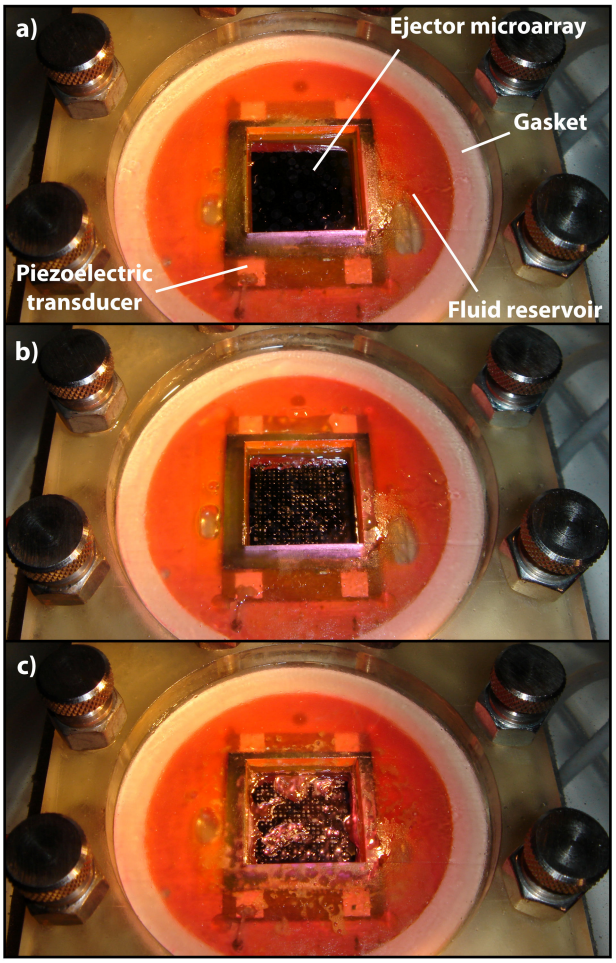

Figure 7. Operation using urethane photopolymer resin: a) Picture of the ejector microarray after cleaning the front face with methanol, b) the microarray immediately after turning on the device (a short burst of ejection was observed lasting approximately 0.5 s), and c) the microarray after a period (~10-15 s) of weeping. Note that in (c) the liquid is very active.

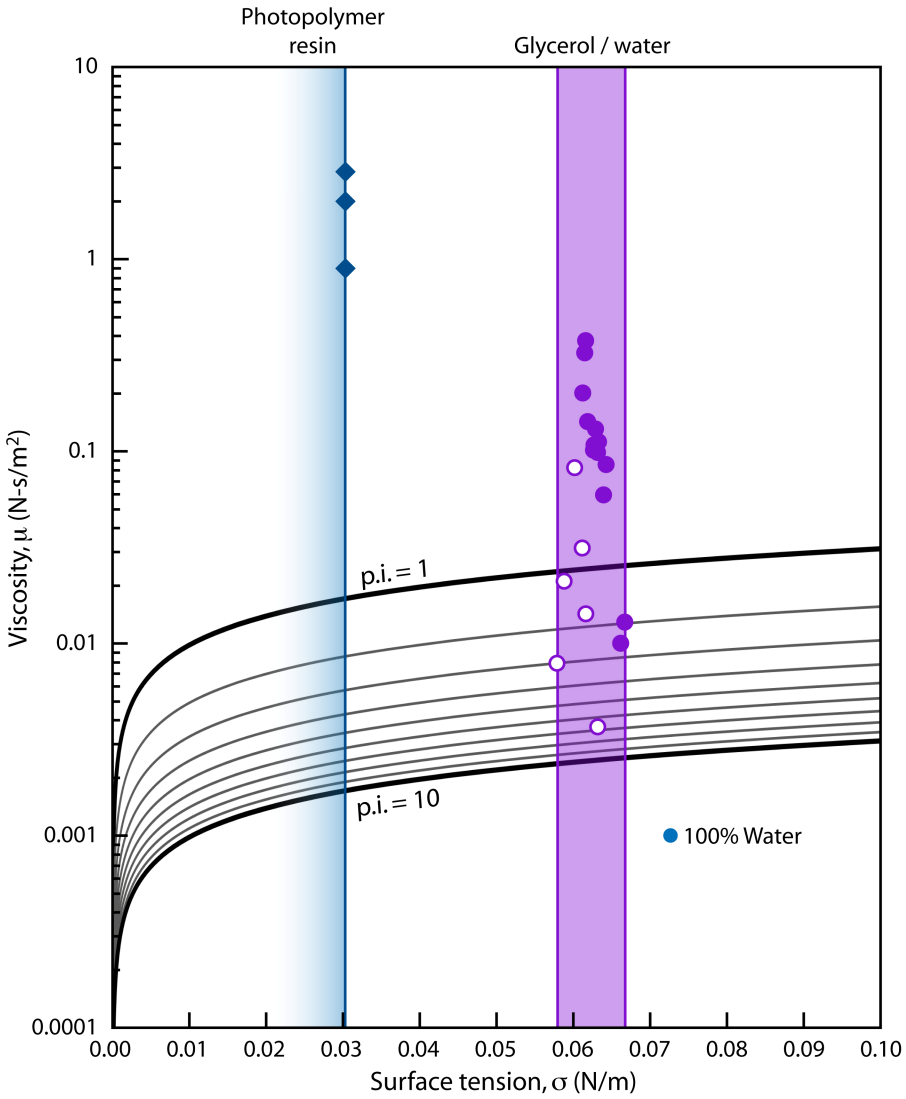

Figure 8. Printing indicator for successfully ejected fluids. Open circles indicate glycerol-water mixtures for which the operating temperature was above 60 °C. All other operating conditions were below 45 °C. Glycerol-water mixtures fall in a surface tension envelope between ~58 and 67 mN/m, while the surface tension of the photopolymer resin is only known to lie below 30 mN/m.

5 Conclusions

We have demonstrated a MEMS-enabled printing technique, which relies on ultrasonic actuation, resonant operation and acoustic wave focusing to produce micro-scale (~50 μm) droplets from a parallel array of pyramidal nozzles. Bulk piezoelectric actuation was used to drive ejection at between 0.5 and 1.0 MHz in order to characterize the acoustic response (and thus resonant behavior) of a 20×20 array of 45 μm side length square orifices etched in a 500 μm thick silicon plate and placed above a 1.5 mm high fluid reservoir. Peaks in the ejection quality were found close to predicted values at frequencies of 550 and 950 kHz. Glycerol-water mixtures and a urethane-based photopolymer resin with a range of properties (surface tensions of ~25–73 mN/m and viscosities of 0.7–3000 mN-s/m^2) were successfully ejected, and the printing capability was evaluated using a qualitative judgment termed ‘jettability’.

The combination of operating parameters realized by the ejector microarray makes possible the deposition of high-viscosity materials that currently cannot be used in printing-based additive manufacturing processes. Because the fundamental physical limits on ejection of high-viscosity fluids are not well understood, the performance envelope of printing such fluids is only loosely defined; thus, development of appropriate ejection technologies has been impeded. Our future efforts will focus on improving device consistency and achieving sustained operation with high-viscosity (> 1000 mN-s/m^2) materials. We will also characterize device operation for fluids with properties that lie between the extremes (low surface tension, high viscosity and high surface tension, low viscosity) presented here.

6 Acknowledgements

The authors would like to express our appreciation for financial support and use of the photopolymer resin with urethane oligomers courtesy of Albany International Research Corporation (Mansfield, MA). We would also like to thank Dr. Victor Breedveld (GT School of Chemical and Biomolecular Engineering, Complex Fluids Group) and Sarp Satir (GT, ME) for assistance in measuring the viscosity and speed of sound, respectively, of the photopolymer resin. All authors were employees at Georgia Tech during the research that led to this paper.

References

1. Calvert, P., *Inkjet printing for materials and devices.* Chemistry Materials, 2001. **13**(10): p. 3299-3305.
2. de Gans, B.-J., P.C. Duineveld, and U.S. Schubert, *Inkjet printing of polymers: state of the art and future developments.* Advanced Materials, 2004. **16**(3): p. 203-213.
3. Sirringhaus, H., et al., *High-resolution inkjet printing of all-polymer transistor circuits.* Science, 2000. **290**(5499): p. 2123-2126.
4. Le, H.P., *Progress and trends in ink-jet printing technology.* Journal of Imaging Science and Technology, 1998. **42**(1): p. pp. 49-62.
5. Jakob, K., et al., *Three-dimensional tissue constructs built by bioprinting.* Biorheology, 2006. **43**(3-4): p. 509-513.
6. Khalil, S., J. Nam, and W. Sun, *Multi-nozzle deposition for construction of 3D biopolymer tissue scaffolds.* Rapid Prototyping Journal, 2005. **11**(1): p. 9-17.
7. Wang, X., Y. Yan, and R. Zhang, *Rapid prototyping as a tool for manufacturing bioartificial livers.* TRENDS in Biotechnology, 2007. **25**(11): p. 505-513.
8. Jakob, K., et al., *Organ printing: Fiction or science.* Biorheology, 2004. **41**(3-4): p. 371-375.
9. Miranov, V., et al., *Organ printing: computer-aided jet-based 3D tissue engineering.* TRENDS in Biotechnology, 2003. **21**(4): p. 157-161.
10. Miranov, V., G. Prestwich, and G. Forgacs, *Bioprinting living structures.* Journal of Materials Chemistry, 2007. **17**(20): p. 2054-2060.
11. Lee, M., J.C.Y. Dunn, and B.M. Wu, *Scaffold fabrication by indirect three-dimensional printing.* Biomaterials, 2005. **26**(20): p. 4281-4289.
12. Cui, T., et al., *Printed polymeric passive RC filters and degradation characteristics.* Solid-State Electronics, 2005. **49**: p. 853-859.
13. Kobayashi, H., et al., *A novel RGB multicolor light-emitting polymer display.* Synthetic Metals, 2000. **111-112**: p. 125-128.
14. Plötner, M., et al., *Investigation of ink-jet printing of poly-3-octylthiophene for organic field-effect transistors from different solutions.* Synthetic Metals, 2004. **147**: p. 299-303.

15. Coakley, K.M. and M.D. McGehee, *Conjugated polymer photovoltaic cells.* Chemistry of Materials, 2004. **16**: p. 4533-4542.
16. Sele, C.W., et al., *Lithography-free, self-aligned inkjet printing with sub-hundred-nanometer resolution.* Advanced Materials, 2005. **17**: p. 997-1001.
17. MacDiarmid, A.G., *Synthetic metals: a novel role for organic polymers.* Synthetic Metals, 2002. **125**: p. 11-22.
18. Ainsley, C., N. Reis, and B. Derby, *Freeform fabrication by controlled droplet deposition of powder filled melts.* Journal of Materials Science, 2002. **37**: p. 3155-3161.
19. Borland, S. and G. Baker, *Method for the construction of an aperture plate for dispensing liquid droplets*, USPTO, Editor. 2001, Aerogen, Inc.: USA.
20. Schuster, J., et al., *The AERX aerosol delivery system.* Pharmaceutical Research, 1997. **14**: p. 354-357.
21. de Heij, B., et al., *Characterization of a fL droplet generator for inhalation drug therapy.* Sensors and Actuators, A, 2000. **85**: p. 430-434.
22. Yuan, S., Z. Zhou, and G. Wang, *Experimental research on piezoelectric array microjet.* Sensors and Actuators, A, 2003. **108**: p. 182-186.
23. Yuan, S., et al., *MEMS-based piezoelectric array microjet.* Microelectronic Engineering, 2003. **66**: p. 767-772.
24. Perçin, G. and B.T. Khuri-Yakub, *Piezoelectrically actuated flextensional micromachined ultrasound droplet ejectors.* IEEE Transactions on Ultrasonics, Ferroelectrics, and Frequency Control, 2002. **49**(6): p. pp. 756-766.
25. Meacham, J.M., et al., *Micromachined ultrasonic droplet generator based on a liquid horn structure.* Review of Scientific Instruments, 2004. **75**(5): p. 1347-1352.
26. Meacham, J.M., et al., *Droplet formation and ejection from a micromachined ultrasonic droplet generator: Visualization and scaling.* Physics of Fluids, 2005. **17**(10): p. 100605-100613.
27. Lide, D.R., *CRC Handbook of Chemistry and Physics*. 86 ed, ed. D.R. Lide. 2005, New York, NY: Taylor & Francis.
28. Miner, C.S. and N.N. Dalton, *Glycerol*. 1953, New York, NY: Reinhold Publishing Corp.
29. Bhagavantam, S. and C.V. Joga Rao, *Ultrasonic velocity and the adiabatic compressibility of some liquids.* Proceedings of the Indian Academy of Sciences, 1939. **9**(4): p. 312-315.
30. Freyer, E.B., J.C. Hubbard, and D.H. Andrews, *Sonic studies of the physical properties of liquids. I. The sonic interferometer. The velocity of sound in some organic liquids and their compressibilities.* Journal of the American Chemical Society, 1929. **51**(3): p. 757-770.
31. Cheng, N.-S., *Formula for the viscosity of glycerol-water mixture.* Industrial and Engineering Chemistry Research, 2008. **47**: p. 3285-3288.
32. Segur, J.B. and H.E. HOberstar, *Viscosity of glycerol and its aqueous solutions.* Industrial and Engineering Chemistry, 1951. **43**(9): p. 2117-2120.
33. Washburn, E.W., C.J. West, and N.E. Dorseay, *International critical tables of numerical data, physics, chemistry, and technology*. 2003, Knovel: Norwich, NY.
34. Chenlo, F., et al., *Kinematic viscosity and water activity of aqueous solutions of glycerol and sodium chloride.* European Food Research and Technology, 2004. **219**(4): p. 403-408.
35. Shankar, P.N. and M. Kumar, *Experimental determination of the kinematic viscosity of glycerol water mixtures.* Proceedings: Mathematical and physical sciences, 1994. **444**(1922): p. 573-581.
36. Harkins, W.D. and F.E. Brown, *The determination of surface tension (free surface energy), and the weight of falling drops: the surface tension of water and benzene by the capillary height method.* Journal of the American Chemical Society, 1919. **41**(4): p. 499-524.

37. Lando, J.L. and H.T. Oakley, *Tabulated correction factors for the drop-weight-volume determination of surface and interfacial tensions.* Journal of Colloid and Interface Science, 1967. **25**(4): p. 526-530.
38. ANSYS, *ANSYS Release 7.1*. 2003, ANSYS, Inc.: Canonsburg, PA, USA.
39. Meacham, J.M., et al., *Micromachined ultrasonic atomizer for liquid fuels.* Atomization and Sprays, 2008. **18**(2): p. 163-190.
40. Jackson, R.G., *Novel Sensors and Sensing*. Series in Sensors, ed. I.o. Physics. 2004, Boca Raton, FL: CRC Press, Taylor and Francis Group.
41. Seerdon, K.A.M., et al., *Ink-jet printing of wax-based alumina suspensions.* Journal of the American Ceramics Society, 2001. **84**: p. 2514-2520.